DOI:10.21715/GB2358-2812.2016301055

Geochronology (U-Pb) and isotope geochemistry (Sr/Sr and Pb/Pb) applied to the Várzea do Capivarita Metamorphic Suite, Dom Feliciano Belt, Southern Brazil: Insights and paleogeographical implications to West Gondwana evolution.

Leonardo Gruber[1]*
Carla Cristine Porcher[2]
Humberto Geller[1]
Luís Alberto D'Ávilla Fernandes[2]
Edinei Koester[2]

[1]Programa de Pós-graduação em Geociências
Instituto de Geociências
Universidade Federal do Rio Grande do Sul
Av. Bento Gonçalves, 9500
Porto Alegre - RS - Brasil
CEP 91501-970.

[2]Departamento de Geologia
Instituto de Geociências
Universidade Federal do Rio Grande do Sul
Av. Bento Gonçalves, 9500
Porto Alegre - RS - Brasil
CEP 91501-970.

*leonardo.gruber@ufrgs.br
carla.porcher@ufrgs.br
humbertogehlen@ig.com.br
ladfernandes@gmail.com
koester@ufrgs.br

*correspondence author

Resumo

Análises geocronológicas e geoquímicas de isótopos nos mármores e gnaisses pelíticos aflorantes na suíte metamórfica Várzea do Capivarita (VCMs) no Cinturão Dom Feliciano (DFB), sul do Brasil, confirma a sua origem durante a aglutinação dos crátons Congo-Kalahari-La Plata no Supercontinente Gondwana, nos períodos Toniano-Criogeniano. Zircão detrítico mostraram proveniência a partir de fontes locais (2,2-2,0 Ga), desde o desenvolvimento de processos de rifteamento (1,7 Ga) e aglutinação de terrenos no Neoproterozóico (0,7 Ga), e restrigem da deposição de sedimentos peliticos dentrode uma idade mínima de 728 ± 11 Ma e idade metamórfica de 618 ± 7,3 Ma. A razão $^{87}Sr/^{86}Sr$ para rocha total de 0,70609 indica uma idade deposição de 717-750 Ma para as sequências de mármore. Dados de $^{206}Pb/^{204}Pb$ e $^{207}Pb/^{204}Pb$ são semelhantes aos obtidos para dolomitos estromatolíticas no Gariep Belt (Kalahari), mas algumass razões são similares às assinaturas dos arcos vulcânicos do Neoproterozóico (ca. 800 Ma) (Cerro Bori Continental Arc) no craton do Rio de La Plata. Metapelitos VCMs podem ser entendidos como sequências de plataformas depositadas durante a aglutinação de terrenos entre cratons Kalahari e do Rio de la Plata, no Neoproterozóico.
Palavras-chave: geoquímica isotópica; Geocronologia; Sturtian Glacial Epoch; Gondwana Ocidental

Abstract

Geochronological and isotope geochemistry analysis on the marbles and pelitic gneisses outcropping in the Várzea do Capivarita Metamorphic Suite (VCMS) in the Dom Feliciano Belt (DFB), Southern Brazil, confirms its origin during the agglutination of Congo-Kalahari-La Plata cratons into the Gondwana Supercontinent, in the Tonian-Cryogenian periods. Detrital zircon ages displayed provenance from local sources (2.2 - 2.0 Ga), from development of rifting processes (1.7 Ga) and agglutination of terranes in the Neoproterozoic (0.7 Ga), and constraint the pelitic sediment deposition within minimum detrital age of 728 ± 11 Ma and metamorphic age of 618 ± 7.3 Ma. Whole-rock $^{87}Sr/^{86}Sr$ ratio of 0.70609 indicates a deposition age of 717 - 750 Ma to the marble sequences. $^{206}Pb/^{204}Pb$ and $^{207}Pb/^{204}Pb$ data are similar to those obtained of stromatolitic dolomites in Gariep Belt (Kalahari) but some ratios are similar to signatures of Neoproterozoic (ca. 800 Ma) volcanic arcs (Cerro Bori Continental Arc) in the Rio de La Plata craton. VCMS metapelites can be understood as plataformal sequences deposited during agglutination of terranes between Kalahari and Rio de La Plata cratons in the Neoproterozoic.
Keywords: Isotope Geochemistry; Geochronology; Sturtian Glacial Epoch; West Gondwana

1. INTRODUCTION

The evolution of West Gondwana supercontinent can be summarized as the result of interactions between five recognized cratons (Amazonia, West African, Rio de La Plata, Kalahari, São Francisco - Congo) and others elusive cratons and terranes, such as Paranapanema and Luis Alvez (Cordani *et al*., 2013) (Fig. 1-a).

The Pan-African-Brasiliano orogeny marks the supercontinent's agglutination on its western side, with consumption of oceanic plates, possibly the Adamastor ocean between Rio de La Plata-Kalahari/Congo, and Khomas Sea between Kalahari/Congo at the end of the Neoproterozoic (e.g Frimmel *et al*., 2008; Basei *et al*., 2011; Rapela *et al*., 2011). In this context, the Dom Feliciano Belt (DFB) in the Southern Brazil is the southernmost portion of the Mantiqueira Province, developed in the aforementioned orogeny. In this context, the Várzea do Capivarita Metamorphic Suite (VCMS) is formed by three roof-pending metasedimentary suites intruded by the Arroio dos Ratos Granitic Complex (Fernandes et al., 1992). These metasedimentary sequences are considered to be the record of a plataformal sequence, with intense metamorphism in the Neoproterozoic (Gross et al., 2006). The depositional ages of these metasedimetary units are considered to be in the Neoproterozoic (Fragoso-César, 1991), which is generally related in a global context to the Sturtian-Cryogenian-Marinoan glacial epochs, recorded by stromatolites and cap carbonates in various geodynamical reconstructions of the Rodínia break-up to the Gondwana assembly.

Trying to constraint depositional ages and provenance of the VCMS, and in this, contextualize the DFB in the Stuartian-Cryogenian-Marinoan glaciations, we used U-Pb in detrital and metamorphic rims of zircon grains of paragneisses, as well as Pb/Pb isotopic ratios and $^{87}Sr/^{86}Sr$ in marbles, aiming to correlate the studied samples with the global registers of Snow Ball Earth (Sturtian Glaciation) and comparison with other sections of DFB and African carbonates.

2. GEOLOGY

The DFB can be subdivided in three major units separated by suture zones (Fernandes *et al*., 1995a,b): (*a)*, Eastern Domain, with post tectonic alkaline granitic intrusions produced mainly in the Neoproterozoic, interpreted as a continental magmatic arc as registered in the Pelotas Batolith (Philipp & Machado, 2005); *(b)*, the Central Domain, whose main feature are schist belts and granitic-gneissic complexes. Schists belts are represented by the Porongos Metamorphic Complex, with provenance ages from ca. 0.5 to 2.8 Ga, with major peaks of U-Pb detrital zircon ages of 2.2 – 2.0 Ga (Basei *et al*., 2011; Gruber *et al*., 2011; Pertille *et al*., 2015a). A TTG-type suite of calc-alkaline gneisses are represented by the Encantadas Complex, which is interpreted as a Paleoproterozoic active continental arc (Philipp *et al*., 2008). Orthogneisses of ca. 630 Ma intrude the paragneisses of the Várzea do Capivarita Metamorphic Suite, outcropping as roof pendant of high grade (amphibolite to granulite facies). These paragneisses are also intruded by calc-alkaline granitoids within mid-crustal mega transcurrent shear zones (Fernandes & Koester, 1999b); and *(c)*, the Western Domain, which is represented by an ophiolite assemblage of a Neoproterozoic juvenile magmatic arc of ca. 750 Ma (Leite *et al*., 1998; Chemale 2000; Saalmann *et al*., 2005; Lena *et al*., 2014), with remnants of older crust that are present in megaxenoliths dated at ca. 0.9 Ga (Hartmann *et al*., 2008) and younger volcanic rocks of post-collisional affinity (Gastal *et al*., 2005).

The VCMS outcrops in the eastern portion of the central domain of the DFB (Fig.1-b). The VCMS is a sequence of metapelites, pure and impure marbles, calc-silicate rocks and mafic gneisses metamorphosed at high-amphibolite to granulite facies (Fernandes *et al*., 1990; Silva *et al*., 2002; Gross *et al*., 2006). Three sections were mapped and classified accordingly to field description, metamorphic association and structural analysis. The three sections are the Arroio Canhão, Cerro Partido and Várzea do Capivarita roof pendants.

The Arroio Canhão roof pendant consists of calc-silicate rocks that shows felsic bands of calcite, quartz, plagioclase, scapolite and K-feldspar, alternating with mafic bands composed of clinopyroxene, biotite and garnet (Silva *et al*., 2002; Gross *et al*., 2006).

The roof pendant of Cerro Partido displays outcrops of pelitic gneisses and migmatitic metapelites. The minimum conditions of metamorphism were estimated with pressures of 3-4 kbar and 730-800ºC,determined in this section by Gross *et al* (2006). These were based on three mineral assemblages: (*i*) garnet–cordierite–spinel–sillimanite–biotite–plagioclase–Kfeldspar in SiO2-poor layers; (*ii*) garnet–quartz–biotite–cordierite–plagioclase–K-feldspar in SiO2-rich layers, and (*iii*) quartz–garnet–biotite–K-feldspar in leucosome layers. In more recent works, the peak conditions were determined as granulite facies (800-850ºC, intermediate pressure and ultra-high temperature series) to the leucogranitic injections in the paragneisses (Bom *et al*., 2014).

The Várzea do Capivarita roof pendant is composed of pure and impure dolomitic marbles. Impure marbles displays centimeter to meter compositional mafic (phlogopite + olivine) and felsic (calcite ± dolomite) layers. Boudins composed of diopside + pargasite interlayered with bands of phlogopite and olivine are common. Pure marbles display massive structures, some of them display original S0 banding preserved, observed in the intercalation of calcitic beds with dolomitic siliceous, quartz-feldspar pelitic gneisses and calc silicate gneisses (Fig. 2-a) (Silva *et al*., 2002; Bom *et al*., 2014). Boudins marked by forsterite encircling dolomite are interpreted as the result of reaction zones generated by hydrothermal fluid percolation (Silva *et al*., 2002).

The metapelites and marbles of VCMS are interpreted as the record of a passive margin, associated with a continental shelf in the Neoproterozoic (Fragoso-César, 1991; Fernandes *et al*., 1992). These sediments were deposited before the amalgamation of the cratons Rio de La Plata and Kalahari/Congo. The metasedimentary pure and impure marbles from VCMS are composed of interlayered bands of calcite and dolomite. Low-Mg calcite and high-Mg dolomites, the later displaying intergrowth with tremolite (Gross *et al*., 2006), were interpreted as product of interaction with hydrothermal fluids enriched in H2O (Silva *et al*., 2002).The high influx of fluids that led to breakdown of biotite and muscovite (Bom *et al*., 2002) and magmatic calc-alkaline intrusions (Cordilheira Granite) suggests that the metapelites and marbles had the peak conditions of metamorphism with intermediate pressures between 6-10 kbar and ultra-high temperature (850-1000º C), possibly as result of a during the apex of the collisional orogenic metamorphism (Silva *et al*., 2002; Bom *et al*., 2014).

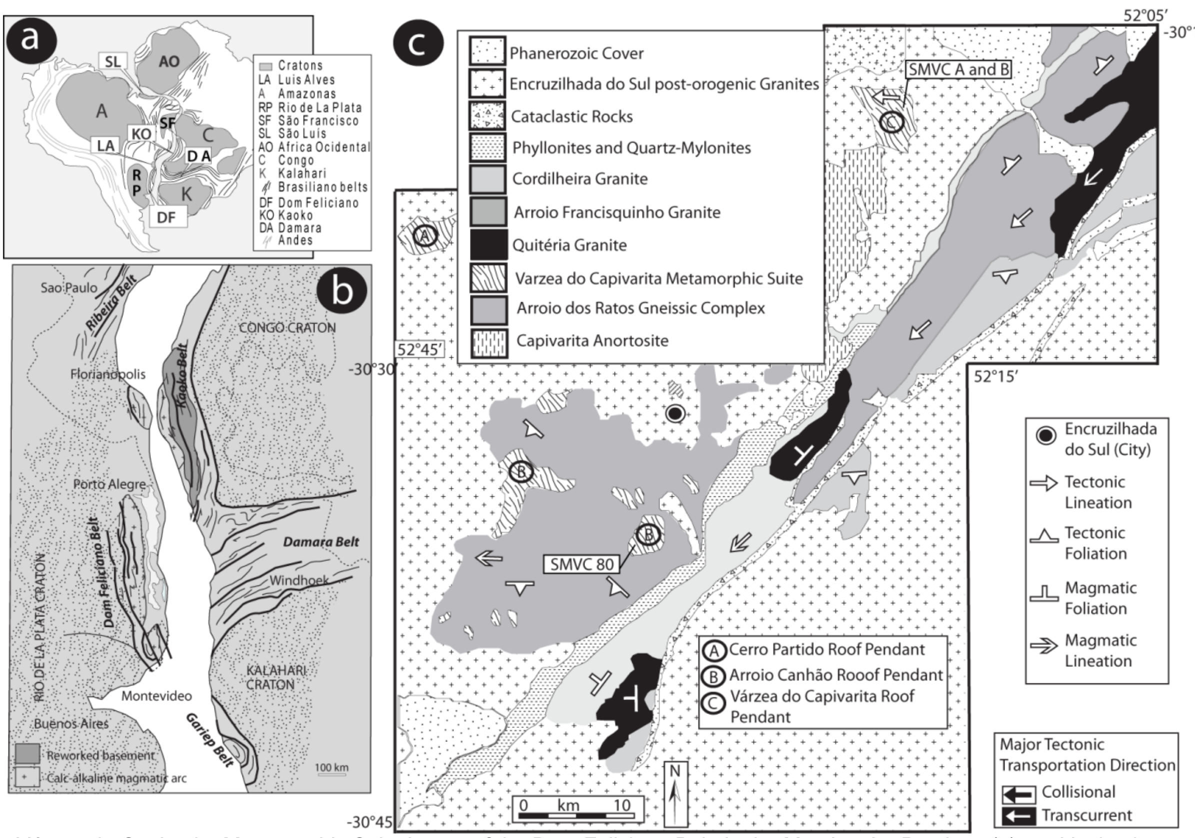

Figure 1 – Várzea do Capivarita Metamorphic Suite is part of the Dom Feliciano Belt, in the Mantiqueira Province (a), and its basin was developed among Kalahary, Congo and Rio de La Plata cratons during Rodínia breakup and Gondwana assembly (b); Geological sketch of the studied area, showing main occurrences of the Várzea do Capivarita Metamorphic Suite outcrops in the Cerro Partido, Arroio Canhão and Várzea do Capivarita roof pendants and localization of selected samples and outcroppings in the VCMS (modified from Silva *et al*., 2002) (c).

3. MATERIALS AND METHODS

Samples (four marbles and three metapelites) were collected in the Arroio Canhão and Várzea do Capivarita roof pendants (Fig.1-b), mainly from a limestone quarry that is characterized by ca. 40 meter walls of marbles interlayered with pelitic gneiss (samples in Fig.2-a and b). Gneiss banding is well marked on outcrop and thin sections in the pelitic gneisses (Fig. 2 –c). Uneven levels of granoblastic quartz-feldspar in alternating bands with biotite in preferred orientation develop an equigranular lepidoblastic texture. Interlobbed contact in quartz grains occurs in the pelitic gneisses.

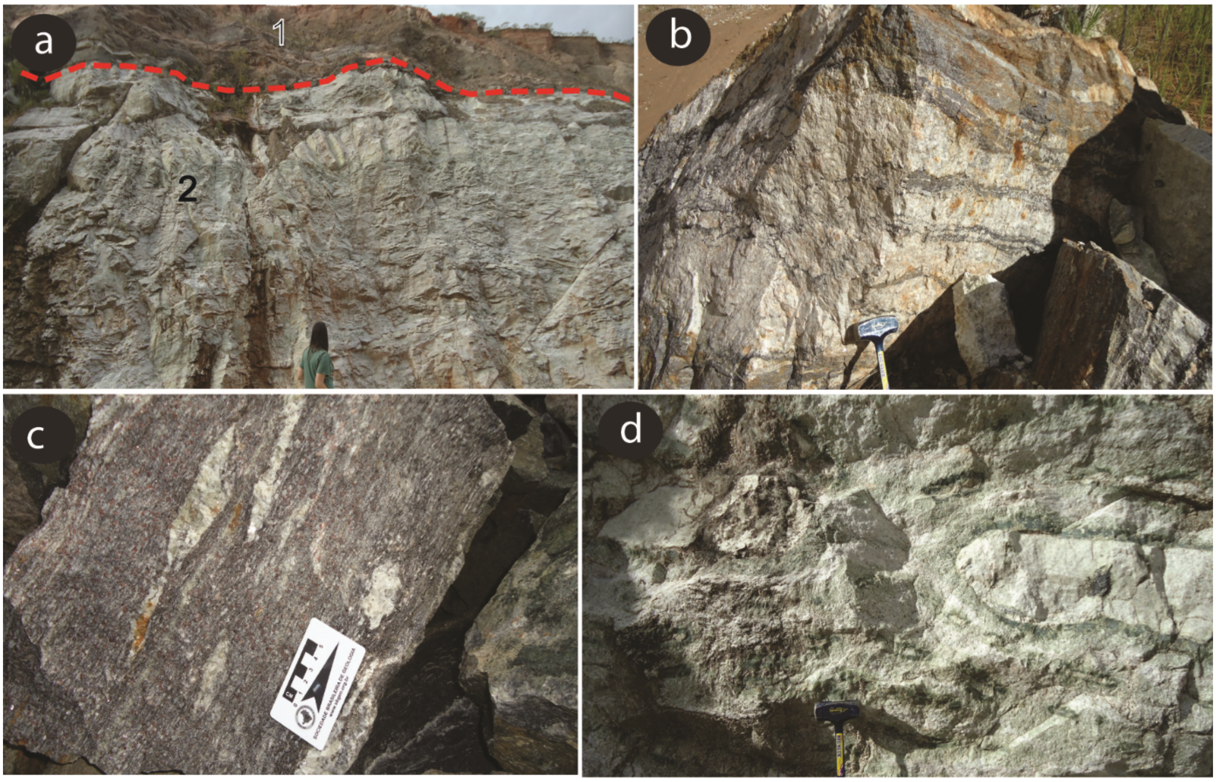

Figure 2 – Várzea do Capivarita Roof Pendant - (a) Marble marking the S0 underlies pelitic, as indicated by dashed line; (b) detail of contact between marble (2) interlayered with pelitic gneiss (1); (c) pinch and swell and boudin textures in the pelitic gneiss; and (d) detail of the marbles.

Whole-rock $^{87}Sr/^{86}Sr$ were analyzed by TIMS using VG SECTOR 54 mass spectrometer at Laboratório de Geologia Isotópica at Federal University of Rio Grande do Sul (LGI-UFRGS). Samples were crushed and pulverized, weighted for ca. 0.01 gr in Savilex® beaks before chemical aperture with lixiviation using HCL 0.25 N at room temperature. Anionic chemical columns LN-B50-A (100 - 200 mesh) and cationic AG-50W-X8 (200 – 400 mesh) were used to separate Rb and Sr, by lixiviation of HCl 2.5N and HNO3 in a step-leeching process. Details in this methodology can be obtained in Bailey *et al* (2000). Results are displayed in Table 1.

For whole-rock Pb isotopic analysis, conventional chromatography cation-exchange methods were used, with dissolution in HNO3 and HF in Savillex® vials. A Finnigan Neptune ICPMS were used for ratio analysis. Uncertainties on $^{207}Pb/^{206}Pb$ are considered better than ± 0.1% (1σ) and ± 0.00001 (1σ), respectively, based on repeated analyses of the BHVO-1 standard. Details about the sample dissolution and analysis parameters can be found in Abre *et al* (2012). Results are presented in Table 2.

Zircon concentrates were extracted from 5-10 kg of rock samples. Samples were crushed in a jaw crusher to a 500 μm size, followed by panning. Zircons were separated by using of standard gravitational techniques and Frantz Isodynamic® separator, and handpicked under binocular microscope. The zircon concentrates were cast in epoxy. Cathodoluminescence images performed prior U-Pb isotopic analyses were used to indicate possible metamorphic rims on the crystal structures (selected images are shown on Figure 3).

U-Pb ages (sample SMVC80) were obtained in the SHRIMP II Centro de Pesquisas Geocronológicas, Geosciences Institute of

Universidade de São Paulo. The analytical procedures used are the same described in Williams (1998). To each zircon grain analyzed, four scans through the mass stations were made for every age determination. Standard Temora 2 with $^{206}Pb/^{238}U$ age of 416.18 ± 0.33 Ma was used to calibrate the $^{206}Pb/^{238}U$ ratios. Decay constants are those recommended by Steiger & Jager (1977). Common lead correction was made with measured ^{204}Pb in each analysis, and data reduction with Squid and Isoplot Excel™ programs (Ludwig, 2003) (Data presented in Tables 3 and 4).

Samples SMVCA and B were dated with laser ablation microprobe (New Wave UP213) coupled to a MC-ICP-MS (ThermoFinnigan-Neptune) at LGI-UFRGS. Isotope data were acquired using static mode with spot size of 25 µm, with frequency of 10 Hz and intensity of ~4 J/cm2. Analyses were made in 40 cycles of 1 s each, with laser-induced elemental fractionation and instrumental mass discrimination corrected by GJ-1 (standard zircon) with the measurement of two GJ-1 analyses to every four sample zircon spots. The external error was calculated after propagation of the error of the GJ-1 mean and the individual sample zircon. Data were reduced using in-house programs developed at the LGI-UFRGS (Results are presented on Tables 5 and 6).

Probability Density Plots and Kernel Density Estimates were made with DensityPlotter (Vermeesch, 2012), with grains with concordance better than 90%, only non-recrystallized nucleus and rims. $^{206}Pb/^{238}U$ ratios were used for Neoproterozoic detrital zircon ages, and $^{206}Pb/^{207}Pb$ to the older grains.

4. RESULTS AND DISCUSSION

4.1. $^{87}Sr/^{86}Sr$

The $^{87}Sr/^{86}Sr$ ratios determined for three of the four marble samples are influenced by their Rb contents and the addition of radiogenic ^{87}Sr (0.7120–0.7152), and therefore are of no further interest to determine depositional features, since these values are affected by post-depositional fluids, forming the paragenesis of Calcite + Dolomite + Olivine as observed by Silva *et al.* (2002). The ratio of 0.70609 was obtained in sample PO-21 is plotted in the secular variation curve for oceans from Jacobsen & Kaufman (1998). We also compare our data to analysis obtained from carbonates and dolomites from African sequences in other works, aiming to determine an approximation to the depositional age of the carbonates and the possible sea isotopic composition, to test if the present data can indeed be interpreted as having a common genesis with other carbonates from the West Gondwana. Considering these $^{87}Sr/^{86}Sr$ ratios and minimum detrital zircon age (see 4.3), the marbles analyzed here could have been deposited at a slighter older age, up to ca. 750 Ma (Fig. 4-a). $^{87}Sr/^{86}Sr$ values of 0.7048 to 0.7063 were obtained by Neis (2014) in the Matarazzo and Fida marbles in Arroio Grande, near the Pinheiro Machado Complex, with granitoids dated of ca. 575 Ma (Philipp *et al.*, 2002) and sin-transcurrent granitoids of ca. 570 Ma (Koester *et al.*, 1997). These carbonates were interpreted in the before mentioned works as having a depositional age of ca. 850 Ma.

In the other hand, marbles and carbonates analyzed in the Passo Feio Formation and in the Cambaí Complex (medium to high grade sequences) near Caçapava granitic intrusion of ca. 560 Ma (Remus *et al.*, 2000a) reveled values of 0.7074 ($^{87}Sr/^{86}Sr$), -0,26‰ and 2.44‰ ($\delta^{13}C_{PDB}$) and -5.68‰ ($\delta^{18}O_{PDB}$) (Passo Feio) 0.7069 ($^{87}Sr/^{86}Sr$), 5.75‰ (δ13CPDB) and -11,64‰ (δ18OPDB) (Cambai Complex). These data confirmed depositional age of 770 - 730 Ma to Passo Feio Formation and 740 - 730 Ma to Cambai Complex (Goulart *et al.*, 2013).

Reconstructions of the Rodínia to Gondwana supercontinent cycles configure Rio de La Plata craton in correlation to Kalahari and Congo cratons in the Mesoproterozoic (McMenamin and McMenamin, 1990) and in the Neoproterozoic (Hartnady *et al.*, 1985; Frimmel 2008; Li *et al.*, 2008). A ^{206}Pb-^{207}Pb age of 728 ± 32 Ma obtained in marbles of the Pickelhaube fm. indicated deposition of ca. 750 Ma, coincident with the glaciation marked in the underlying Stinkinfontein Subgroup (Fölling *et al.*, 2000). These data are registered as the post-rift evolution in the Gariep Belt, and can be used as parameter to compare marbles from Rio de La Plata side of the pre-Gondwana assemble to African side, notably those found on Damara, Namaqua-Natal and Gariep belts. $^{87}Sr/^{86}Sr$ ratios of the Widouw Formation (Namaqua-Natal Belt) were found varying from 0.7082 to 0.7085 in the Bloeddrif Member (Gariep) and 0.7080 to 0.7087 in the Kombuis member (Saldania Belt) (Frimmel 2008), all of those higher than that found in this work and in other comparable sections of DFB.

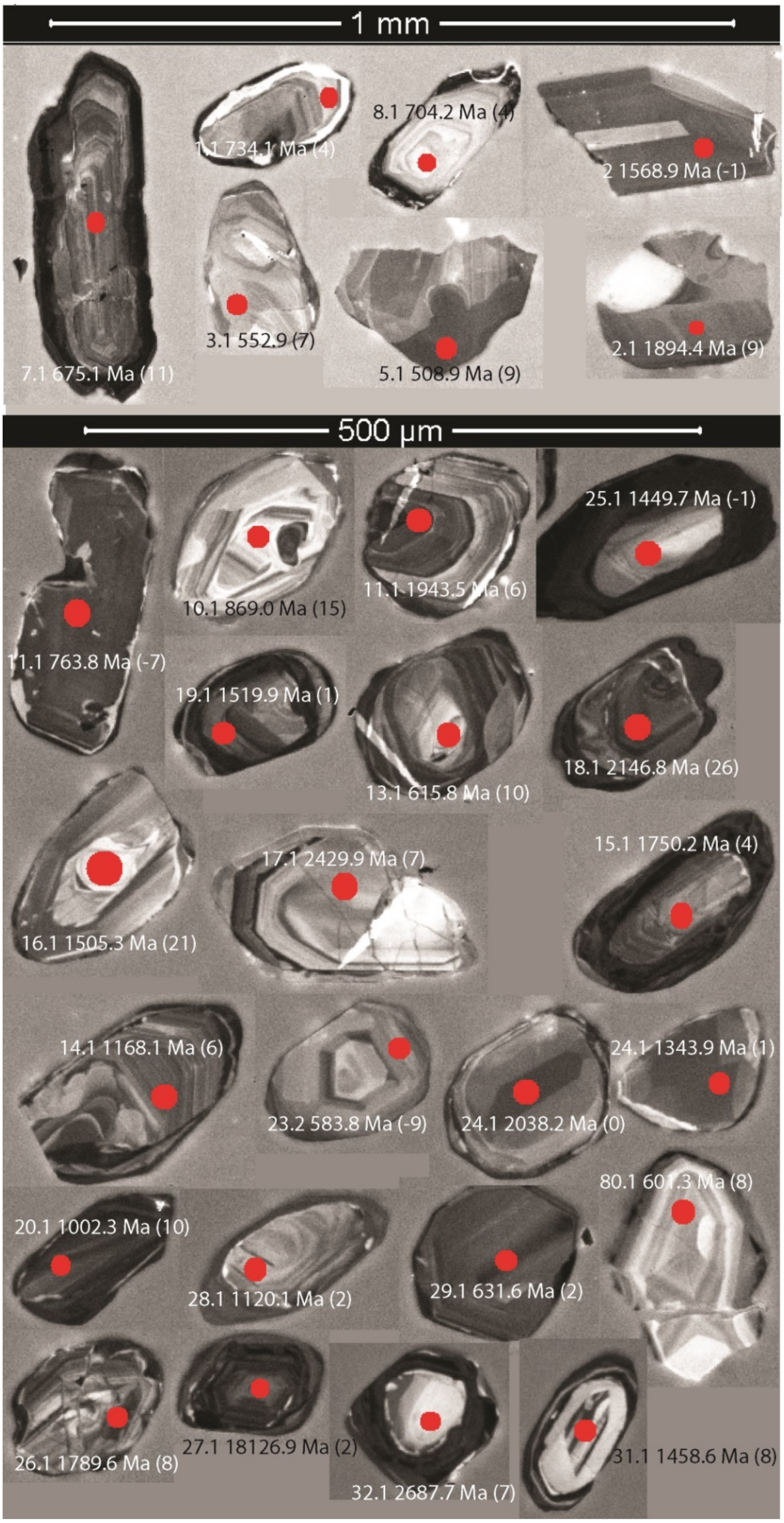

Figure 3 - Selected cathodoluminescence images for sample SMVC80 (red circle indicates beam position; includes ages and analysis number for reference). Cathodoluminescence imaging was carried out using a scanning electron microscope at the Universidade de São Paulo, Brazil.

Geodynamical reconstruction of Rodínia configuration is displayed in Fig.6, to show possible correlation of the sea level and isotopic variations at ca. 715-750 Ma. Considering the preliminary data presented here, the values of marbles from Cambaí Complex (São Gabriel Block or western DFB), Passo Feio Formation (Western DFB) and Matarazzo and Fida marbles (Eastern DFB) (Fig. 4-a) can be used as a proxy to estimate the depositional age of VCMS marbles. The estimative of a pre-Cryogenian age to the deposition of these marbles could represent a correlation tool with others marble and carbonate sequences originated in the Sturtian glacial epoch (Rooney *et al.*, 2015). The studied marbles underwent high-temperature and low-pressure metamorphism (see section 2), obliterating any petrological or facies association to recognize cap carbonates typical from glaciation periods (e.g. Hoffman *et al.*, 1998; Fairchild, 1993).

4.2. Pb-Pb

The analyzed samples displayed values of $^{207}Pb/^{204}Pb$ varying from 25.08 to 17.92, $^{206}Pb/^{204}Pb$ varying from 15.56 to 16.13 and $^{208}Pb/^{206}Pb$ varying from 37.57 to 38.04. The uranogenic values varied within the domains of typical samples of Pan-African signatures and Rio de La Plata signatures (e.g. Oyhantçabal *et al.*, 2011), with values of $^{206}Pb/^{204}Pb$ 15.56 and $^{208}Pb/^{206}Pb$ 37.57 plotting close to those obtained in the Cerro Bori orthogneisses (Lenz *et al.*, 2012) and Porongos Metamorphic Complex schists (Gruber *et al.*, 2016a) (Fig. 5-a), and this variation on the values obtained could be due to metasomatism affecting the samples. Alternatively, the terrigenous materials in the marbles could record varied degrees of dispersion of the uranogenic values, so it's not reasonable to predict source-areas in this manner. Nonetheless, thoro-uranogenic values displayed samples plotting near those values obtained in the Gariep samples of Frimmel & Föelling (2004) (Fig.5-b). In this manner, it is interpreted here that the uranogenic values indicates that the deposition of VCMS marbles was in an ocean between Rio de La Plata and Kalahari cratons in the Neoproterozoic, thus supporting the suggested paleogeography (Fig. 6) of a plataformal sequence, as suggested by Fragoso-César (1991). This ocean can be represented by the Adamastor Ocean (Hartnady *et al.*, 1995), or a series of small seas between arcs and terranes, as constrained in models from Frimmel *et al.* (2011). Considering the reported $^{87}Sr/^{86}Sr$ ratios and U-Pb ages (see 4.3), it's possible to admit this sea would represent the initial rifting phase of the Brazilides Ocean

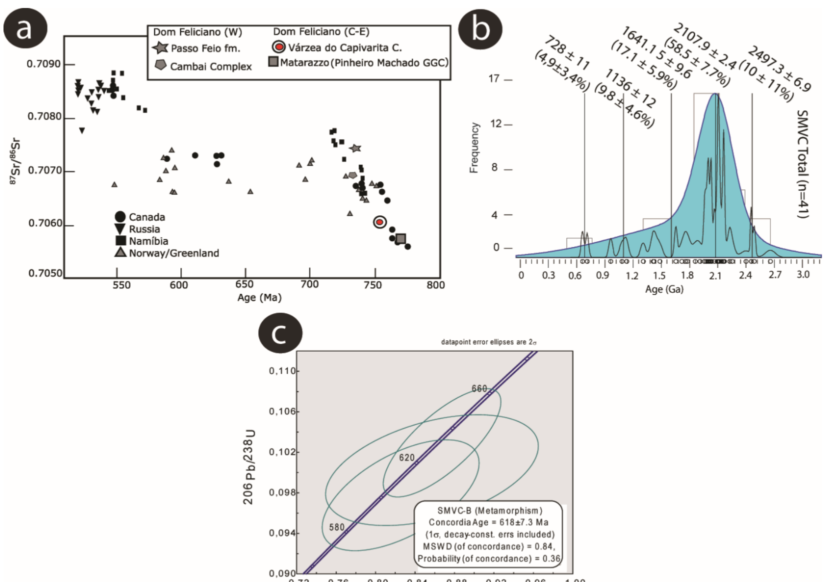

Figure 4 – (a) - $^{87}Sr/^{86}Sr$ temporal and spatial variation of carbonates and evaporites from various units used to define the principal glaciations of the Neoproterozoic (modified from Jacobsen and Kaufman, 1998; Frimmel 2008, Goulart *et al.*, 2011, Neis 2014); Stacked distribution ages for VCMS (b); metamorphic Concordia age for the sample SMVCB found in zircons with typical metamorphic growth textures (c).

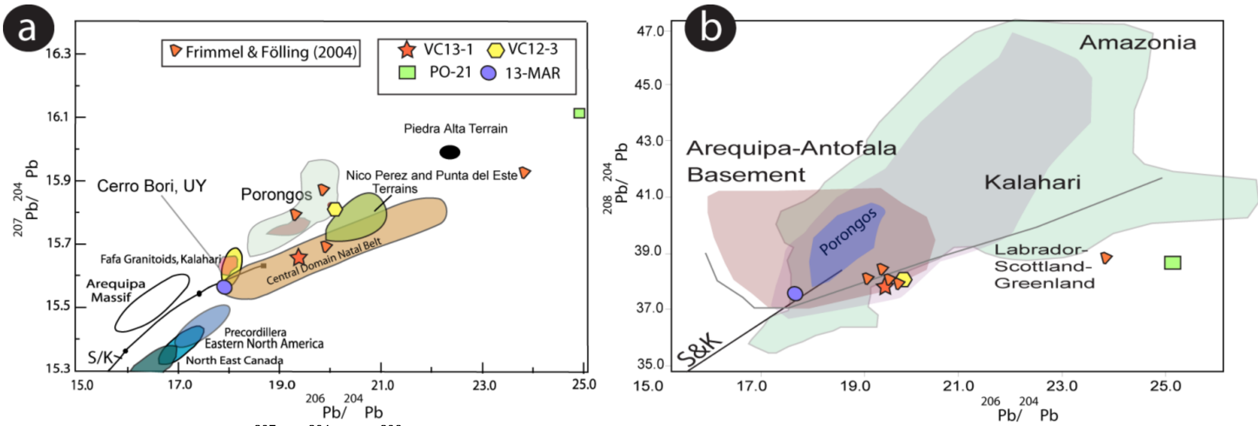

Figure 5 - (a) Uranogenic ^{207}Pb/^{204}Pb x ^{206}Pb/204Pb analysis plotted in comparison with samples from Kalahari, Congo, N. America and Cerro Bori Continental Arc (localized in the Dom Feliciano Belt, Uruguay); Porongos Metamorphic Complex schists and quartzites, Punta Del Este and Piedra Alta Terrane, and stromatolitic dolomites from Marmora Terrane, in the Pan-African Gariep Bel; samples from VCMS displays similar patterns to some of the dolomites of the Gariep belt, as well as some relation to metassediments of Porongos Metamorphic Complex and Nico Pérez Terrane. The high variability of VCMS marbles could be interpreted as varied degree of metassomatism affecting the samples; nonetheless, they all plot near values obtained to DFB and its African counterpart; (b) Thorogenic ^{208}Pb/^{204}Pb X ^{206}Pb/^{204}Pb, displaying a congruence between the analysed samples and samples from Gariep Belt; in this case, Porongos Metamorphic Complex schists didn't displayed proximal values to those found to VCMS. Modified from Oyhantçabal *et al*. (2011). Data from Cerro Bory presented by Lenz *et al.* (2012), data from Porongos Metamorphic Complex from Gruber *et al.* (2016) and Gariep Belt samples from Frimmel & Föelling (2004); S&K evolution curve from two stage model's evolution of Stacey & Kramers (1975).

4.3. U-Pb

Three samples (SMVC A, SMVC B and SMVC80) were analyzed and have its results presented and discussed here. From the 20 grains from metapelitic gneiss SMVCA and 64 grains of SMVCB, 28.1 ± 8.2 % of the total have an estimated age of 2140.8 ± 54 Ma. Sample SMVC80 displayed roughly the same patterns. Concordance better than 90 are found in 41 analyzed grains and are discussed below.

Including all samples, the probability density presented five optimal clusters (detrital zircons dated only): 1 – A cluster with 4.9 ± 3.4% of detrital zircon grains presented a maximum depositional age of 728 ± 11 Ma, which can be roughly related to the estimated depositional age for the marbles, and correlates well with depositional ages obtained for the Pickelhaube Formation and Stinkinfontein Subgroup (see item above) and the base of the glaciogenic Grand Conglomerate on Congo craton (Rooney *et al*., 2015). Since the analyzed marbles occur intercalated with banded gneisses, the S0 from the metapelites can be understood as a minimum depositional age for the marbles as well; 2 – A second cluster is in the same age ranges found in PMC's schists of ca. 1.2 Ga (Basei *et al*., 2011; Gruber *et al*., 2011; Pertille *et al*., 2015a and b). This cluster can be correlated with Stenian to early Tonian sources and represents 9.8 ± 4.6% of the total detrital record, with an estimated age of 1136 ± 12 Ma; 3 - this cluster (17.1 ± 5.9%) indicates an source-terrane with an age of 1641.1 ± 9.6 Ma, and could be related to the Capivarita Anorthosite and other Pan-African sources with ages between 1.3-1.5 Ga, related to extensional settings on the margin of Congo craton (Mayer *et al*., 2004; Chemale *et al*., 2011); clusters 4 and 5 represents another local source of 2107.9 ± 2.4 (58.5 ± 7.7% of total data), and the oldest zircon grains dated in these three samples with ages varying from 2.4 to 2.0 Ga, possibly representing detrital material from Encantadas Complex and Neto Rodrigues Orthogneiss (Remus *et al*., 2000a). The histograms of stack probability density age distribution are shown in Figure 4-b.

Metamorphic rims were detected in zircon ribbons, and were used to calculate a Concordia age of 618 ± 7.3 Ma (Fig. 4-c) to SMVCB, and better constraint the high-temperature and low-pressure metamorphism S1 placed by Sm-Nd garnet-whole rock ages of 626-604 Ma obtained in the same rocks by Gross *et al* (2006). This metamorphic zircon age is in the same range of ages obtained in zircon's rims crystalized under partial melting conditions in migmatites from the Florianópolis Batolith, located at the northern tip of the DFB (Silva et al., 2005). This is a further evidence for the extension of DFB orogeny's continental mature arc setting in the Neoproterozoic.

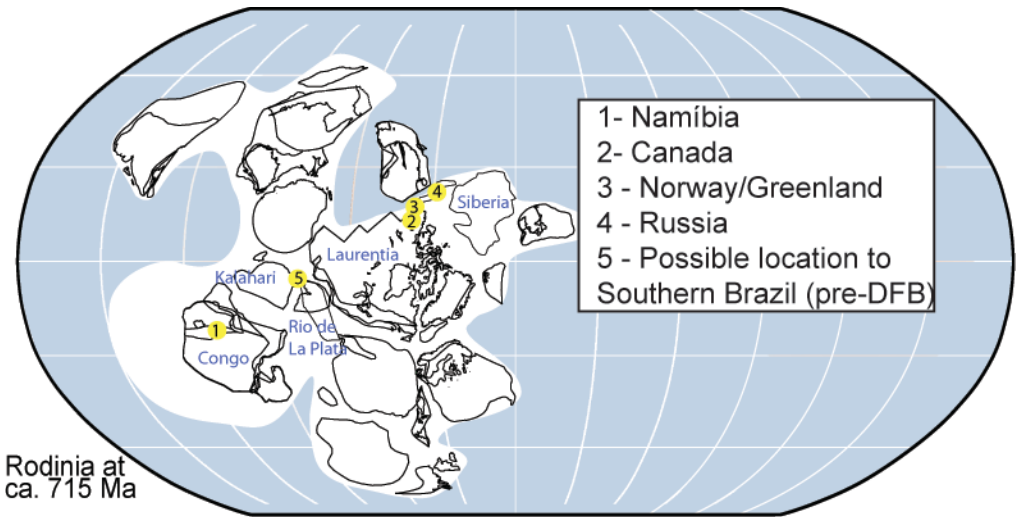

Figure 6 - Reconstruction of Rodínia supercontinent at ca. 715 Ma (modified from Rooney *et al*., 2015, using the reconstruction of Li *et al*., 2013). Considering that DFB were developed between Rio de La Plata and Kalahari cratons, we estimated a possible position of the VCMS pelagic basin in the Rodínia break-up scheme.

5. CONCLUSIONS

The metamorphic record is constrained between 625 to 610 Ma (considering the uncertainty in the age of 618 ± 7.3 Ma), marking an orogenic event, likely related to the collision of the reworked margins of Rio de La Plata and Kalahari cratons. Comparison with Porongos Metamorphic Complex metasediments and the basement rocks in the DFB indicates that the same patterns of Mesoproterozoic and Paleoproterozoic provenance is registered with VCMS metasediments. However, maximum and minimum depositional ages for VCMS are older than those obtained in the PMC. PMC is interpreted as an Ediacaran basin (Pertille *et al*., 2015b), so they could not represent the same depositional setting. The origin of the clusters with same ages can be explained by reworking of the same source-terranes in the transition from passive margin to collisional setting at ca. 600 Ma.

VCMS pelitic gneisses have a maximum depositional age of 728 ± 11 Ma to the original pelitic sequences and ca. 717-750 Ma to the marble sequences, which could be interpreted as a record of a plataformal marine environment in the West Gondwana agglutination context. Future works in the marbles and carbonates in the DFB should evaluate the possible correlation of these units and the Stuartian glacial epoch.

6. ACKNOWLEDGEMENT

We would like to thank the Agência Nacional do Petróleo, Gás Natural e Biocombustíveis (ANP), Financiadora de Estudos e Projetos (FINEP) and Ministério da Ciência e Tecnologia (MCT), (PRH-ANP/MCT), Petrobras PRH-PB215 for studentship (first author) and the LGI-UFRGS staff for providing analysis and technical support. Also, we'd like also to thank Prof. Dr. Márcio Martins Pimentel for providing help with analysis, and thanks GB editor Profa. Dra. Valderez Ferreira and an anonymous reviewer for the insightful comments on an early draft of the manuscript.

Table 1 – Whole-rock $^{87}Sr/^{86}Sr$ Data (Várzea do Capivarita Roof Pendant marbles).

Sample	$^{87}Sr/^{86}Sr$	error (%)	N. of Analysis
VC 13-1	0.71527912	0.0021	80
13-Mar	0.71268259	0.0014	100
VC 12-03	0.71204570	0.0028	80
PO 21	0.70609164	0.0006	100

Table 2 – Whole-rock Pb/Pb Data (Várzea do Capivarita Roof Pendant marbles).

Sample Name	$^{206}Pb/^{204}Pb$	SE (%)	$^{207}Pb/^{204}Pb$	SE (%)	$^{208}Pb/^{204}Pb$	SE (%)
VC13-1	19.4212	0.003483	15.651667	0.002915	37.613468	0.006895
13/mar	17.9252	0.003756	15.567244	0.003200	37.573106	0.007532
VC12-03	20.3793	0.003914	15.790098	0.003454	38.046486	0.008872
PO21	25.0805	0.009486	16.131532	0.006070	37.743674	0.014223

Table 3 – Zircon U-Th-Pb SHRIMP Data (sample SMVC80 - Arroio Canhão Roof Pendant).

Spot	$^{204}Pb/^{206}Pb$	%err	$^{207}Pb/^{206}Pb$	%err	$^{208}Pb/^{206}Pb$	%err	%comm 206	ppm U	ppm Th	$^{232}Th/^{238}U$
1-1.1	7.6E-4	26	.075	2.6	.142	3.0	1.42	186	75	0.42
1-2.1	3.1E-4	33	.132	0.9	.173	1.1	0.59	145	82	0.58
1-3.1	3.0E-4	50	.064	1.7	.157	1.5	0.56	294	135	0.47
1-4.1	4.3E-4	25	.065	1.6	.462	0.9	0.81	344	492	1.48
1-5.1	3.3E-4	24	.063	1.4	.106	1.5	0.61	506	161	0.33
1-6.1	3.2E-4	25	.068	2.2	.086	1.8	0.61	376	86	0.24
1-7.1	6.9E-4	18	.074	1.5	.204	1.2	1.30	335	192	0.59
1-8.1	4.2E-4	31	.070	1.4	.116	1.5	0.78	303	102	0.35
1-9.1	6.2E-5	43	.128	0.6	.232	0.7	0.12	312	239	0.79
1-10.1	4.4E-4	24	.079	1.4	.078	1.9	0.82	297	44	0.15
1-11.1	2.9E-4	26	.067	1.4	.300	1.0	0.55	355	341	0.99
1-12.1	1.7E-4	79	.104	1.1	.171	1.2	0.32	288	83	0.30
2-13.1	5.3E-4	25	.070	2.6	.276	1.8	0.99	264	208	0.81
3-14.1	3.0E-4	23	.086	1.1	.083	2.4	0.55	262	65	0.26
3-15.1	1.5E-4	32	.113	1.2	.189	1.4	0.28	179	112	0.65
3-16.1	6.3E-4	21	.120	1.0	.272	0.9	1.18	187	150	0.83
3-17.1	2.7E-4	24	.178	0.8	.164	1.1	0.51	126	71	0.59
3-18.1	1.1E-4	29	.187	0.7	.139	1.5	0.21	326	152	0.48
3-19.1	1.8E-4	23	.098	0.7	.099	1.0	0.33	473	151	0.33
4-20.1	5.7E-5	15	.077	1.0	.065	1.7	0.11	424	83	0.20
4-21.1	2.7E-4	29	.103	2.4	.035	7.8	0.51	189	12	0.06
4-21.2	1.1E-4	23	.116	0.6	.024	2.3	0.20	548	60	0.11
4-22.1	5.4E-5	60	.127	0.9	.209	0.7	0.10	299	212	0.73
4-23.1	1.7E-4	97	.068	2.7	.236	2.3	0.32	163	115	0.73
4-24.1	1.2E-4	43	.089	1.0	.384	0.7	0.23	279	349	1.29
4-23.2	5.1E-4	49	.065	3.0	.202	1.7	0.96	194	116	0.62
4-25.1	7.2E-4	25	.101	1.7	.389	1.3	1.35	74	92	1.29
5-26.1	2.2E-4	20	.122	0.7	.279	1.4	0.41	277	248	0.93
5-27.1	1.1E-4	32	.115	0.6	.201	0.7	0.21	396	259	0.67
5-28.1	2.5E-4	27	.081	1.2	.159	1.2	0.46	244	110	0.46
5-29.1	2.0E-4	27	.064	1.1	.410	0.7	0.37	569	739	1.34
5-30.1	4.0E-4	24	.067	1.6	.223	1.2	0.75	327	218	0.69
6-31.1	4.0E-4	16	.103	0.8	.252	0.9	0.75	294	191	0.67
6-32.1	1.4E-4	60	.206	1.0	.282	2.0	0.26	63	61	1.00

Table 4 - SHRIMP ages (sample SMVC80).

Spot	^{204}corr ^{206}Pb /2^{38}U Age	1s err	^{207}corr ^{206}Pb /2^{38}U Age	1s err	^{208}corr ^{206}Pb /^{238}U Age	1s err	^{204}corr ^{207}Pb /^{206}Pb Age	1s err	^{204}corr ^{208}Pb /2^{32}Th Age	1s err	% Dis-cor-dant
1-1.1	731.4	15.7	730.8	16.0	736.1	16.8	750	124	656	53	3
1-2.1	1894.4	36.6	1862.1	42.5	1899.2	39.8	2071	27	1833	65	9
1-3.1	552.9	12.2	552.1	12.3	552.9	13.1	594	90	553	27	7
1-4.1	568.9	12.0	569.0	12.2	571.8	15.8	563	77	558	14	-1
1-5.1	508.9	11.7	508.2	11.8	511.0	12.3	554	58	468	21	9
1-6.1	578.8	12.0	576.2	12.2	578.7	12.5	705	68	582	31	22
1-7.1	675.1	14.0	673.1	14.3	676.0	15.5	753	85	665	27	11
1-8.1	704.2	14.6	703.4	14.9	706.5	15.4	732	76	661	39	4
1-9.1	1943.5	35.9	1919.9	42.1	1941.0	40.2	2066	12	1966	45	6
1-10.1	869.0	17.8	864.0	18.4	862.9	18.4	1002	59	1145	90	15
1-11.1	753.8	15.4	755.4	15.9	759.0	18.2	699	53	722	19	-7
1-12.1	1043.3	21.2	1007.1	22.0	1006.6	22.6	1649	41	1876	76	58
2-13.1	615.8	13.1	614.5	13.4	613.5	15.1	675	99	633	22	10
3-14.1	1168.1	23.3	1163.8	24.6	1170.7	24.3	1240	36	1098	56	6
3-15.1	1750.2	45.6	1741.0	51.8	1753.3	50.1	1815	25	1716	59	4
3-16.1	1505.3	33.7	1471.4	36.8	1500.5	38.6	1815	41	1545	54	21
3-17.1	2429.9	57.7	2361.5	77.5	2439.7	62.4	2600	17	2300	81	7
3-18.1	2146.8	39.1	1982.6	52.3	2148.2	41.8	2700	12	2123	59	26
3-19.1	1519.9	29.0	1517.8	31.9	1522.6	30.4	1541	19	1462	44	1
4-20.1	1002.3	19.9	997.8	20.7	1001.6	20.5	1098	21	1029	29	10
4-21.1	835.3	17.7	801.2	18.4	833.3	17.9	1611	52	1048	162	93
4-21.2	1421.1	27.0	1375.4	29.2	1429.8	27.4	1870	12	848	51	32
4-22.1	2038.2	37.3	2036.7	45.3	2040.3	41.3	2046	16	2018	47	0
4-23.1	607.0	13.3	602.4	13.4	605.3	15.0	807	97	621	27	33
4-24.1	1343.9	26.2	1342.7	28.3	1346.2	32.4	1359	26	1333	31	1
4-23.2	583.8	15.2	584.9	15.4	585.6	16.7	529	164	566	36	-9
4-25.1	1449.7	31.3	1451.0	34.1	1460.9	38.7	1436	72	1395	48	-1
5-26.1	1789.6	33.9	1766.8	38.6	1786.4	39.1	1936	17	1813	48	8
5-27.1	1812.6	34.8	1807.1	40.1	1810.6	38.4	1848	14	1834	45	2
5-28.1	1120.1	27.4	1119.1	28.9	1114.5	29.6	1138	37	1202	41	2
5-29.1	631.6	12.8	631.4	13.1	635.1	16.2	643	40	617	14	2
5-30.1	601.3	13.1	600.3	13.4	602.3	14.8	647	69	593	19	8
6-31.1	1458.6	28.0	1446.8	30.5	1430.7	31.6	1582	29	1742	46	8
6-32.1	2687.7	52.8	2579.3	81.1	2683.1	60.8	2864	18	2723	91	7

Table 5 - Laser Ablation ICP-MS U–Pb data (MT110 – SMVCA; MT109 – SMVCB) (Várzea do Capivarita Roof Pendant pelitic gneiss).

Sample	f(206)%	Th/U	6/4 ratio	7/6 ratio	1s(%)	7/5 ratio	1s(%)	6/8 ratio	1s(%)	Rho
03_mt110_1	0.09	0.38	181375	0.06373	6.2	0.9432	6.6	0.10734	2.2	0.33
04_mt110_2	0.02	0.29	295326	0.13377	1.8	6.2664	2.3	0.33975	1.4	0.61
05_mt10_3	0.04	0.43	113172	0.06212	2.6	0.8561	2.8	0.09996	1.1	0.37
06_mt110_04	0.02	0.21	256747	0.06266	3.8	0.8716	3.9	0.10089	1.1	0.45
09_mt110_05	0.01	0.43	1576	0.13751	2.1	7.0993	2.8	0.37443	1.8	0.65
10_mt110_6	0.03	0.64	4077	0.05808	3.2	0.8043	3.5	0.10044	1.3	0.36
11_mt110_7	0.01	0.51	11368	0.12476	1.8	5.0388	2.2	0.29292	1.2	0.53
12_mt110_08	0.02	0.47	1104	0.06235	3.7	0.8278	3.9	0.09629	1.2	0.45
15_mt110_09	0.02	0.36	4799	0.11813	4.0	2.3975	4.3	0.14719	1.5	0.34
16_mt110_10	0.06	0.29	570	0.13114	1.4	5.7211	1.9	0.31640	1.2	0.63
17_mt110_11	0.03	0.27	5505	0.05763	2.5	0.8339	3.0	0.10495	1.7	0.54
18_mt110_12	0.07	0.09	12113	0.06142	11.8	0.9036	12.0	0.10671	2.3	0.35
22_mt110_13	0.00	0.38	181375	0.09734	1.2	1.9344	2.4	0.14413	2.1	0.86
23_mt110_14	0.01	0.29	295326	0.10370	1.4	2.1844	2.2	0.15278	1.8	0.78
18_mt110_15	0.01	0.43	113172	0.09991	11.6	2.4082	16.7	0.17482	12.0	0.72
25_mt110_16	0.01	0.21	256747	0.10151	2.1	2.5974	2.9	0.18559	1.9	0.85
26_mt110_17	0.00	0.43	1576	0.13366	1.1	5.3695	1.9	0.29136	1.6	0.81
29_mt110_18	0.02	0.64	4077	0.05947	1.5	0.8287	1.8	0.10107	1.0	0.53
30_mt110_19	0.00	0.51	11368	0.13061	3.1	3.6168	6.7	0.20084	5.9	0.89
30_mt110_20	0.01	0.47	1104	0.07356	1.5	1.1965	1.8	0.11797	1.0	0.72
34_mt110_21	0.01	0.36	4799	0.11003	1.0	3.6822	1.6	0.24272	1.2	0.76
29_mt110_18	0.01	0.29	570	0.13054	0.9	5.4477	1.4	0.30267	1.1	0.75
36_mt110_23	0.00	0.27	5505	0.07847	1.3	1.3201	1.6	0.12201	1.0	0.59
37_mt110_24	0.01	0.09	12113	0.06828	8.1	0.7941	8.9	0.08435	3.6	0.66
40_mt110_25	0.00	0.38	181375	0.13220	0.9	6.3027	1.4	0.34579	1.0	0.73
41_mt110_26	0.01	0.29	295326	0.08731	2.7	1.6930	4.7	0.14064	3.9	0.82
42_mt110_27	0.01	0.43	113172	0.06035	0.9	0.8677	1.4	0.10429	1.0	0.71
43_mt110_28	0.00	0.21	256747	0.13704	2.5	5.3860	2.9	0.28505	1.5	0.73
11_mt109_5	0.04	0.35	29560	0.06426	0.9	0.8800	1.2	0.09932	0.8	0.64
12_mt109_6	0.05	0.13	37098	0.13570	0.8	7.3937	1.2	0.39517	0.9	0.74
14_mt109_8	0.01	0.25	9987	0.15660	0.7	7.4745	1.1	0.34617	0.9	0.86
17_mt109_9	0.01	0.45	83536	0.13101	0.5	4.6915	1.7	0.25971	1.6	0.94
19_mt109_11	0.01	0.30	24008	0.12739	0.6	5.0234	2.4	0.28599	2.4	0.97
20_mt109_12	0.02	0.30	33258	0.12581	0.8	5.2948	1.6	0.30523	1.3	0.92
23_mt109_13	0.20	0.40	33753	0.06019	2.5	0.7821	2.9	0.09425	1.5	0.50
24_mt109_14	0.01	0.23	31043	0.13767	0.5	7.0410	0.9	0.37095	0.7	0.81
25_mt109_15	0.04	0.20	33824	0.13388	0.6	7.6517	1.4	0.41453	1.3	0.92
35_mt109_21	0.03	0.21	38344	0.06112	1.0	0.8927	1.1	0.10593	0.6	0.51
36_mt109_22	0.03	0.22	56341	0.13275	0.6	6.7264	1.2	0.36749	1.1	0.88
41_mt109_25	0.03	0.31	30808	0.12468	0.6	6.6758	1.2	0.38832	1.0	0.85
43_mt109_27	0.03	0.32	47022	0.13322	0.6	7.7572	1.7	0.42232	1.5	0.93
44_mt109_28	0.03	0.23	38594	0.13019	1.7	5.5539	2.0	0.30940	1.0	0.73
47_mt109_29	0.02	0.33	32670	0.12526	0.5	5.7846	1.1	0.33493	1.0	0.89
53_mt109_33	0.02	0.18	20079	0.12980	0.6	7.0792	2.3	0.39557	2.2	0.97
54_mt109_34	0.21	0.23	82526	0.05970	1.8	0.9601	2.5	0.11664	1.8	0.70
55_mt109_35	0.02	0.31	55610	0.11663	0.6	3.6503	1.6	0.22699	1.5	0.94
56_mt109_36	0.01	0.30	14914	0.11378	1.0	3.7389	1.3	0.23833	0.9	0.81
60_mt109_37	0.02	0.35	29560	0.11755	1.2	3.8465	3.9	0.23733	3.7	0.95
61_mt109_38	0.01	0.13	37098	0.06834	1.6	0.9902	2.7	0.10508	2.2	0.80
62_mt109_39	0.07	0.13	18379	0.06013	1.0	0.8802	1.5	0.10616	1.1	0.72
63_mt109_40	0.02	0.25	9987	0.16595	0.8	10.3187	1.2	0.45097	1.0	0.87
66_mt109_42	0.03	0.31	27997	0.13780	0.6	7.8436	1.1	0.41282	0.9	0.84
67_mt109_43	0.03	0.30	24008	0.13689	0.5	7.7536	1.5	0.41080	1.4	0.93
73_mt109_47	0.04	0.20	33824	0.13063	0.6	6.0723	1.5	0.33715	1.4	0.92

Table 5 -Continuation

Sample	f(206)%	Th/U	6/4 ratio	7/6 ratio	1s(%)	7/5 ratio	1s(%)	6/8 ratio	1s(%)	Rho
74_mt109_48	0.04	0.25	68167	0.13216	1.0	7.0739	1.3	0.38820	0.9	0.82
78_mt109_50	0.05	0.25	30257	0.10357	0.8	4.2852	1.2	0.30008	0.9	0.76
79_mt109_51	0.01	0.23	48280	0.11069	0.5	4.3217	1.1	0.28318	1.0	0.88
80_mt109_52	0.06	0.32	40790	0.05872	6.1	0.7942	7.6	0.09809	4.5	0.82
86_mt109_56	0.02	0.30	57776	0.12346	0.6	5.5794	1.5	0.32777	1.4	0.92
89_mt109_57	0.03	0.36	51106	0.12145	0.8	3.8525	1.4	0.23006	1.1	0.88
89_mt109_57	0.03	0.31	30808	0.12161	0.6	3.8478	1.3	0.22947	1.1	0.86
91_mt109_59	0.02	0.32	47022	0.14218	1.7	6.5227	3.7	0.33273	3.3	0.89
95_mt109_61	0.04	0.33	32670	0.12704	0.6	5.8914	1.2	0.33633	1.0	0.87
97_mt109_63	0.04	0.34	43095	0.06023	0.8	0.8574	1.2	0.10324	0.9	0.73
98_mt109_64	0.01	0.27	39232	0.12567	1.4	4.4589	2.7	0.25733	2.3	0.94
102_mt109_65	0.03	0.18	20079	0.12451	0.6	4.7964	1.4	0.27938	1.3	0.89
103_mt109_66	0.05	0.23	82526	0.12034	0.5	5.1493	1.4	0.31035	1.3	0.92
104_mt109_67	0.02	0.31	55610	0.12764	0.5	6.5324	1.9	0.37119	1.8	0.96
105_mt109_68	0.02	0.30	14914	0.12647	0.9	6.6125	1.4	0.37922	1.1	0.87
108_mt109_69	0.01	0.35	29560	0.14461	1.7	8.1139	4.0	0.40694	3.7	0.91
109_mt109_70	0.04	0.13	37098	0.12236	0.6	6.1634	1.6	0.36532	1.5	0.93
114_mt109_72	0.01	0.45	83536	0.12484	0.8	4.7699	2.0	0.27712	1.8	0.91
115_mt109_74	0.02	0.31	27997	0.12851	0.5	4.8857	1.3	0.27573	1.2	0.91
116_mt109_75	0.01	0.30	24008	0.16286	0.5	9.3016	1.7	0.41424	1.6	0.96
120_mt109_77	0.01	0.40	33753	0.13323	0.7	8.0394	3.3	0.43765	3.3	0.98
121_mt109_78	0.01	0.23	31043	0.14248	1.2	8.7441	3.1	0.44511	2.9	0.92
123_mt109_80	0.23	0.25	68167	0.06681	4.2	0.9601	4.5	0.10422	1.6	0.59

Table 6- Laser Ablation ICP-MS U–Pb ages (MT110 – SMVCA; MT109 – SMVCB) (Várzea do Capivarita Roof Pendant pelitic gneiss).

Sample	7/6 age	1s(Ma)	7/5 age	1s(Ma)	6/8 age	1s(Ma)	Conc (%)
03_mt110_1	732.7	132.0	674.6	32.6	657.3	13.7	89.71
04_mt110_2	2148.1	30.8	2013.8	19.7	1885.4	22.9	87.77
05_mt10_3	678.1	55.5	628.0	13.2	614.2	6.3	90.56
06_mt110_04	696.7	80.0	636.4	18.6	619.6	6.8	88.94
09_mt110_05	2196.1	36.6	2124.0	24.8	2050.2	31.9	93.36
10_mt110_6	532.6	70.2	599.2	15.6	617.0	7.6	115.84
11_mt110_7	2025.4	32.5	1825.9	18.5	1656.1	17.3	81.76
12_mt110_08	686.2	78.5	612.4	17.8	592.7	6.7	86.37
15_mt110_09	1928.1	71.7	1241.8	30.6	885.2	12.3	45.91
16_mt110_10	2113.3	25.3	1934.6	16.4	1772.1	19.0	83.86
17_mt110_11	515.7	55.4	615.8	13.9	643.3	10.1	124.74
18_mt110_12	653.8	253.8	653.7	58.1	653.6	14.1	99.97
22_mt110_13	1573.8	23.3	1093.1	16.3	868.0	17.0	55.15
23_mt110_14	1691.3	25.5	1176.1	15.6	916.5	15.1	54.19
18_mt110_15	1622.4	216.2	1245.1	119.9	1038.6	115.2	64.02
25_mt110_16	1651.8	38.7	1299.9	21.0	1097.4	19.7	66.44
26_mt110_17	2146.6	19.5	1880.0	16.6	1648.3	23.1	76.79
29_mt110_18	584.3	31.7	612.9	8.1	620.7	5.8	106.22
30_mt110_19	2106.2	54.4	1553.2	53.2	1179.8	63.9	56.02
30_mt110_20	1029.3	30.7	799.0	9.9	718.9	6.5	69.84
34_mt110_21	1799.9	18.2	1567.5	12.5	1400.8	15.2	77.83
29_mt110_18	2105.2	15.8	1892.4	12.0	1704.5	15.9	80.97
36_mt110_23	1158.9	25.2	854.6	9.3	742.1	6.9	64.04
37_mt110_24	877.1	168.3	593.5	40.0	522.1	18.1	59.52
40_mt110_25	2127.3	15.9	2018.8	11.9	1914.5	16.7	89.99
41_mt110_26	1367.4	51.9	1005.9	30.3	848.3	31.0	62.04

Table 6 -Continuation

Sample	7/6 age	1s(Ma)	7/5 age	1s(Ma)	6/8 age	1s(Ma)	Conc (%)
42_mt110_27	616.0	20.3	634.3	6.4	639.5	6.0	103.81
43_mt110_28	2190.1	43.2	1882.6	25.1	1616.7	22.1	73.82
11_mt109_5	750.3	18.6	641.0	5.6	610.4	4.6	81.35
12_mt109_6	2173.0	14.0	2160.2	11.1	2146.8	17.2	98.79
14_mt109_8	2419.3	11.4	2169.9	9.9	1916.3	14.6	79.21
17_mt109_9	2111.6	9.6	1765.7	13.8	1488.4	20.7	70.48
19_mt109_11	2062.3	10.4	1823.3	20.7	1621.5	34.0	78.62
20_mt109_12	2040.2	14.9	1868.0	13.4	1717.2	20.0	84.17
23_mt109_13	610.3	53.1	586.7	12.7	580.6	8.1	95.14
24_mt109_14	2198.0	8.2	2116.6	7.7	2033.9	12.7	92.53
25_mt109_15	2149.4	9.7	2190.9	12.8	2235.6	24.7	104.01
35_mt109_21	643.6	20.4	647.8	5.5	649.1	4.0	100.84
36_mt109_22	2134.7	9.9	2076.1	10.8	2017.6	18.8	94.52
41_mt109_25	2024.3	11.0	2069.4	10.8	2115.0	18.9	104.48
43_mt109_27	2140.8	10.3	2203.3	14.8	2271.0	29.5	106.08
44_mt109_28	2100.5	29.9	1909.0	17.0	1737.7	15.4	82.73
47_mt109_29	2032.5	8.3	1944.1	9.5	1862.2	15.9	91.62
53_mt109_33	2095.2	10.2	2121.4	20.2	2148.6	40.2	102.55
54_mt109_34	592.8	38.1	683.4	12.4	711.2	11.9	119.97
55_mt109_35	1905.2	10.1	1560.6	12.9	1318.7	18.2	69.21
56_mt109_36	1860.6	17.2	1579.7	10.3	1378.0	10.7	74.06
60_mt109_37	1919.3	21.4	1602.5	31.3	1372.8	45.6	71.53
61_mt109_38	878.9	32.9	698.8	13.6	644.1	13.3	73.28
62_mt109_39	608.3	22.6	641.1	7.3	650.4	7.0	106.93
63_mt109_40	2517.2	12.9	2463.8	11.4	2399.6	19.3	95.33
66_mt109_42	2199.8	9.6	2213.2	9.7	2227.8	17.3	101.27
67_mt109_43	2188.2	9.5	2202.8	13.4	2218.6	25.9	101.39
73_mt109_47	2106.4	10.4	1986.3	13.3	1872.9	22.9	88.91
74_mt109_48	2126.8	16.9	2120.8	11.9	2114.5	16.5	99.42
78_mt109_50	1689.1	13.9	1690.5	9.9	1691.7	14.0	100.16
79_mt109_51	1810.7	9.4	1697.5	9.2	1607.3	14.0	88.77
80_mt109_52	556.9	133.5	593.6	34.0	603.2	25.7	108.31
86_mt109_56	2006.8	10.4	1912.9	13.0	1827.5	22.1	91.07
89_mt109_57	1977.6	15.0	1603.8	11.4	1334.8	13.6	67.50
89_mt109_57	1980.0	11.1	1602.8	10.3	1331.7	13.4	67.26
91_mt109_59	2253.9	28.9	2049.0	32.5	1851.6	53.0	82.15
95_mt109_61	2057.4	9.9	1960.0	10.3	1869.0	17.0	90.84
97_mt109_63	611.9	17.7	628.7	5.8	633.4	5.6	103.52
98_mt109_64	2038.3	25.5	1723.4	22.7	1476.2	30.7	72.42
102_mt109_65	2021.9	11.3	1784.3	11.9	1588.2	17.7	78.55
103_mt109_66	1961.2	9.7	1844.3	12.0	1742.4	19.9	88.84
104_mt109_67	2065.7	8.6	2050.3	16.3	2035.0	31.2	98.51
105_mt109_68	2049.4	16.3	2061.0	12.4	2072.6	18.7	101.13
108_mt109_69	2283.1	28.6	2243.8	36.5	2200.9	68.7	96.40
109_mt109_70	1990.9	10.4	1999.3	14.0	2007.3	25.7	100.82
114_mt109_72	2026.5	14.2	1779.6	16.6	1576.8	25.2	77.81
115_mt109_74	2077.7	9.1	1799.8	10.8	1569.8	16.3	75.56
116_mt109_75	2485.5	8.4	2368.2	15.8	2234.3	31.0	89.89
120_mt109_77	2141.0	12.6	2235.5	30.1	2340.1	63.9	109.30
121_mt109_78	2257.5	20.6	2311.7	28.3	2373.5	56.9	105.14
123_mt109_80	832.0	87.8	683.3	22.4	639.1	9.6	76.81

7. REFERENCES

Abre, P., Cingolani, C.A., Cairncross, B., Chemale Jr., F. 2012. Siliciclastic Ordovician to Silurian units of the Argentine Precordillera: Constraints on provenance and tectonic setting in the proto-Andean margin of Gondwana. *Journal of South American Earth Sciences* 40, 1-22.

Bailey, T.R., McArthur, J.M., Prince, H., Thirlwall, M.F. 2000. Dissolution methods for strontium isotope stratigraphy: whole rock analysis. *Chemical Geology*, **167 (3-4)**, 313-319

Basei, M.A.S., Campos Neto, M.C., Castro, N.A., Nutman, A.P., Wemmer, K., Yamamoto, M.T., Hueck, M., Osako, L., Siga, O., Passarelli, C.R. 2011. Tectonic evolution of the Brusque Group, Dom Feliciano belt, Santa Catarina, Southern Brazil. *Journal of South American Earth Sciences*, **32**, 24-350.

Bom, F.M., Philipp, R.P., Zvirtes, G. 2014. Evolução metamórfica e estrutural do Complexo Várzea do Capivarita, Cinturão Dom Feliciano, Encruzilhada do Sul, RS. *Pesquisas em Geociências*, **41 (2)**, 131-153.

Chemale, F. 2000. Evolução Geológica do Escudo Sul-rio-grandense. In: Holz, M.; De Ros, L. F. (eds.). *Geologia do Rio Grande do Sul*. Porto Alegre, CIGO/UFRGS, p. 13-52.

Chemale, F., Philipp, R.P., Dussin, I.A., Formoso, M.L.L., Kawashita, K., Bertotti, A.L. 2011. Lu-Hf and U-Pb age determination of Capivarita Anorthosite in the Dom Feliciano Belt, Brazil. *Precambrian Research*, **186**, 117-126.

Cordani, U.G., Pimentel, M.M., Araújo, C. E. G., Fuck, R. A. 2013. The significance of the Transbrasiliano-Kandi tectonic corridor for the amalgamation of West Gondwana. *Brazilian Journal of Geology*, **43**(3): 583-597, doi:110.5327/Z2317-48892013000300012.

Fairchild, I.J., 1993. Balmy shores and ice wastes: the paradox of carbonates associated with glacial deposits in Neoproterozoic times. *Sedimentology Review* **1**, 1-16.

Fernandes, L.A.D., Tommasi, A., Porcher, C.C. 1990. Esboço estrutural de parte do Batólito de Pelotas - região de Quitéria-Capivarita. *Acta Geologica Leopoldensia*, **13**, 117–138.

Fernandes L.A.D., Tommasi A., Porcher C.C. 1992. Deformation patterns in the Southern Brazilian Branch of the Pan-African Dom Feliciano belt. *Journal of South American Earth Sciences*., 5:77-96

Fernandes L.A.D., Menegat R., Costa A.F.U., Koester E., Kramer G., Tommasi A., Porcher, C.C., Ramgrab G.E., Camozzato E. 1995a. Evolução tectônica do Cinturão Dom Feliciano no Escudo Sul-rio-grandense: Parte I - uma contribuição a partir do registro geológico. *Revista Brasileira de Geociências*, **25**, 351-374

Fernandes, L.A.D., Menegat, R., Costa, A.F.U., Porcher, C.C., Tommasi, A., Kraemer, G., Rambgrab, G.E., Camozzato, E. 1995b. Evolução tectônica do Cinturão Dom Feliciano no Escudo Sul-riograndense: uma contribuição a partir das assinaturas geofísicas. *Revista Brasileira de Geociências*, **25**, 375–384.

Fernandes, L.A.D., Koester, E. 1999. The Neoproterozoic Dorsal de Canguçu Strike-Slip Shear Zona: its nature and role in the tectonic evolution of southern Brazil. *Journal of African Earth Sciences*, **29**, 3-24.

Fragoso-César, A. R. S. 1991. *Tectônica de Placas no Ciclo Brasiliano: As Orogenias dos Cinturões Dom Feliciano e Ribeira no Rio Grande do Sul.* Tese de Doutorado, USP, São Paulo. 367 p.

Frimmel, H.E., Basei, M.S., Gaucher, C. 2011. Neoproterozoic geodynamic evolution of SW Gondwana: a southern African perspective. *Int J Earth Sci (Geol Rundsch)*, **100**, pp. 323–354.

Frimmel, H.E. 2008. An evaporitic facies in Neoproterozoic post-glacial carbonates: The Gifberg Group, South Africa. *Gondwana Research,* **13**, 453–468

Frimmel, H.E. and Föelling, P.G. 2004. Late Vendian Closure of the Adamastor Ocean: Timing of Tectonic Inversion and Syn-orogenic Sedimentation in the Gariep Basin *Gondwana Research*, **7**, pp. 685-699.

Fölling, P.G., Zartman, R.E., Frimmel, H.E., 2000. A novel approach to doublespike Pb–Pb dating of carbonate rocks: examples from Neoproterozoic sequences in southern Africa. *Chemical Geology*, **171,** 97–122.

Gastal, M.C.P., Lafon, J.M., Hartmann, L.A., Koester, E., 2005. Sm–Nd isotopic com-positions as a proxy for magmatic processes during the Neoproterozoic of thesouthern Brazilian shield. *Journal of South American Earth Sciences,* **18**, 255–276.

Goulart, R.V., Remus, M.V.D., Reis, R. S. 2013. Composição isotópica de Sr, C e O e geoquímica de ETRs das rochas carbonáticas do Bloco São Gabriel, Rio Grande do Sul. *Pesquisas em Geociências*, **40 (1)**: 75-97.

Gross, A.O.M.S., Porcher C.C., Fernandes L.A.D., Koester E. 2006. Neoproterozoic low pressure/high-temperature collisional metamorphic evolution in the Varzea do Capivarita Metamorphic Suitee, SE Brazil: thermobarometric and Sm/Nd evidence. *Precambrian Research*, **147**, 41–64.

Gruber, L., Porcher, C. C., Lenz, C., Fernandes, L.A.D. 2011. Proveniência de metassedimentos das sequências Arroio Areião, Cerro Cambará e Quartzo Milonitos no Complexo Metamórfico Porongos, Santana da Boa Vista, RS. *Pesquisas em Geociências*, **38**, n.1: 205-224.

Gruber, L., Porcher, C.C., Koester, E., Bertotti, A.L., Lenz, C., Fernandes, L.A.D., Remus, M.V.D., 2016. Isotope geochemistry and geochronology of syndepositional volcanism in Porongos

Metamorphic Complex, Santana da Boa Vista antiform, Dom Feliciano Belt, Brazil: Onset of an 800 Ma continental arc. *Journal of Sedimentary Environments,* **1(2)**: 202-221.

Hartnady, C., Joubert, P., Stowe, C. 1985. Proterozoic crustal evolution in southwestern Africa. *Episodes* **8**:236–244.

Hoffman, P.F., Kaufman, A.J., Halverson, G.P. & Schrag, D.P., 1998. A Neoproterozoic snowball Earth. *Science* **281**, 1342-46.

Jacobsen, S.B and Kaufman, A.J. 1999. The Sr, C and O isotopic evolution of Neoproterozoic seawater. Chemical *Geology*, **161**: 37–57.

Koester, E., Soliani, E. Jr., Fernandes, L.A.D., Kraemer, G., Tommasi, A. 1997. Geocronologia Rb/Sr e K/Ar dos granitóides sintectônicos á Zona de Cisalhamento Transcorrente Dorsal de Canguçu na região de Encruzilhada do Sul (RS). *Pesquisas*, **24**:67–77.

Leite, J.A.D., Hartmann, L.A., Fernandes, L.A.D., McNaughton, N.J., Soliani Jr., E., Koester, E., Santos, J.O.S., Vasconcellos, M.A.Z., 1998. Zircon U–Pb zircon geochronology of Neoproterozoic juvenile and crustal reworked terranes in southernmost Brazil. *Int. Geol. Rev.* **40**, 688–705.

Lena, L.O.F., Pimentel, M.M., Philipp, R.P., Armstrong, R., Sato, K. The evolution of the Neoproterozoic São Gabriel juvenile terrane, southern Brazil based on high spatial resolution U-Pb ages and $\delta^{18}O$ data from detrital zircons. *Precambrian Research*, **247**, 126-138.

Lenz, C.C., Porcher, C.C., Fernandes, L.A.D., Masquelin, H., Koester, E., Conceição, R.V. 2012 Geochemistry of the Neoproterozoic (800–767 Ma) Cerro Bori orthogneisses, Dom Feliciano Belt in Uruguay: tectonic evolution of an ancient continental arc. *Mineralogy and Petrology*, 107(5):785-806.

Li, Z.X., Bogdanova, S.V., Collins, A.S., Davidson, A., De Waele, B., Ernst, R.E., Fitzsimons ICW, Fuck, R.A., Gladkochub, D.P., Jacobs, J., Karlstrom, K.E., Lu, S., Natapov, L.M., Pease, V., Pisarevsky, S.A., Thrane, K., Vernikovsky, V. 2008. Assembly, configuration, and break-up of Rodinia: a synthesis. *Precambrian Research*, **160**:179–210

Li, Z.X., Evans, D.A.D., and Halverson, G.P. 2013. Neoproterozoic glaciations in a revised global paleogeography from the breakup of Rodinia to the assembly of Gondwanaland: *Sedimentary Geology*, **294**, 219–232, doi:10.1016/j.sedgeo.2013.05.016.

Ludwig, K.R. 2003. Isoplot 3.0 – A geochronological toolkit for Microsoft Excel. Berkley Geochronology Center, *Special Publications* **No. 4**.

Mayer, A., Hoffmann, A.W., Sinigoi, S., Morais, E. 2004. Mesoproterozoic Sm-Nd and U-Pb ages for the Kunene Anorthosite Complex of SW Angoa. *Precambrian Research*, **133** (3-4), 187-206.

McMenamin, M.A.S., McMenamin, D.L.S. 1990. **The emergence of animals: the Cambrian breakthrough**. Columbia University Press, New York

Neis,L. 2013. Geoquímica de metacarbonatos do escudo Sul-Rio-Grandense na região de Caçapava do Sul e Arroio Grande, RS. . Unpublished undergraduate dissertation, 61 pp. Universidade Federal do Rio Grande do Sul.

Oyhantçabal P., Siegesmund S., Wemmer K., Layer P. 2010. The Sierra Ballena Shear Zone in the southernmost Dom Feliciano Belt (Uruguay): evolution, kinematics and deformation conditions. *International Journal of Earth Sciences (Geol. Rundschau)* **v. 99**: 1227–1246.

Oyhantçabal, P., Siegesmund, S., Wemmer, K. 2011. The Rio de la Plata Craton: a review of units, boundaries, ages and isotopic signature. *International Journal of Earth Science*, 100, 201–220.

Pertille, J., Hartman, L.A., Philipp, R.P. 2015a. Zircon U-Pb age constraints on the Paleoproterozoic sedimentary basement of the Ediacaran Porongos Group, Sul-Riograndense Shield, southern Brazil. *Journal of South American Earh Sciences* 63, pp.334-345.

Pertille, J., Hartmann, L.A., Philipp, R.P., Petry, T.S., Lana, C.C. 2015b. Origin of the Ediacaran Porongos Group, Dom Feliciano Belt, southern Brazilian Shield, with emphasis on whole rock and detrital zircon geochemistry and U-Pb, Lu-Hf isotopes. *Journal of South American Earth Sciences* 64, pp. 69-93.

Philipp, R.P., Machado, R., Nardi, L. V. S., Lafon, J.M. 2002. O magmatismo granítico Neoproterozóico do Batólito Pelotas no Sul do Brasil: Novos dados e revisão da geocronologia regional. *Revista Brasileira de Geociências*, **32** (2), pp. 277-290.

Philipp, R.P. & Machado, R. 2005. The Neoproterozoic to Cambrian Granitic Magmatism of Pelotas Batholith, Southern Brazil. *Journal of South American Earth Sciences* 19, 461-478.

Philipp, R.P., Lusa, M., Nardi, L. 2008. Petrology of dioritic, tonalitic and trondhjemitic gneisses from Encantadas Complex, Santana da Boa Vista, southernmost Brazil: Paleoproterozoic continental-arc magmatism. *Anais da Academia Brasileira de Ciências*, **80**, n.4.

Rapela, C.W., Fanning, C.M., Casquet, C., Pankhurst, R.J., Poiré, L.S.D. Baldo, E.G. 2011. The Rio de la Plata craton and the adjoining Pan-African/brasiliano terranes: Their origins and incorporation into south-west Gondwana, *Gondwana Research*, **(20):4**, p. 673-690.

Remus, M.V.D., Hartmann, L.A., McNaughton, N.J., Groves, D.I., Fletcher, I.R., 2000a. The link between hydrothermal epigenetic copper mineralization and the Caçapava Granite of the Brasiliano Cycle in southern Brazil. *Journal of South American Earth Sciences*, **13**, 191– 216.

Rooney, A.D., Strauss, J.V., Brandon, A.D., Macdonald, F.A. 2015. A Cryogenian chronology: Two long-lasting synchronous Neoproterozoic glaciations. *Geology*, **43**, 459-462. doi:10.1130/G36511.1.

Saalmann, K., Hartmann, L.A., Remus, M.V.D., Koester, E., Conceição, R.V., 2005. Sm–Nd isotope geochemistry of metamorphic volcanosedimentary successions in the São Gabriel Block, southernmost Brazil: evidence for the existence ofjuvenile Neoproterozoic oceanic crust to the east of the Rio de la Plata craton. *Precambrian Research*, **136**, 159–175.

Saalmann, K., Gerdes, A., Lahaye, Y., Hartmann, L.A., Remus, M.V.D., Läufer, A., 2011. Multiple accretion at the eastern margin of the Rio de la Plata craton: the prolonged Brasiliano orogeny in southernmost Brazil. *International Journal of Earth Sciences,* **100**, 355–378.

Silva, A.O.M.S., Porcher, C.C., Fernandes, L.A.D., Droop, G.T.R. 2002. Termobarometria da Suíte Metamórfica Várzea do Capivarita (RS): Embasamento do Cinturão Dom Feliciano. *Revista Brasileira de Geociências*, **32 (4)**: 419-432.

Silva, L.C., McNaughton, N.J., Flecther, I.R. 2005. SHRIMP U-Pb geochronology of Neoproterozoic crustal granitoids (Southern Brazil): A case of discrimination of emplacement and inherited ages. Lithos, **82**, 503-525.

Stacey, J.S & Kramers, J.D. 1975. Approximation of a terrestrial lead isotope evolution by a two-stage model. *Earth and Planetary Science Letters*, **26**, 207-221.

Steiger., R.H., Jäger, E. 1977. Subcommission on geochronology: convention on the use of decay constants in geo- and cosmochronology. *Earth and Planetary Science Letters* **36**, 359–362.

Vermeesch, P., 2012. On the visualisation of detrital age distributions. *Chemical Geology*, **v.312-313**, 190-194, doi: 10.1016/j.chemgeo.2012.04.021

Williams, I.S. 1998. U-Th-Pb Geochronology by Ion Microprobe. In McKibben, M. A., Shanks III, W. C., and Ridley, W. I. (eds.): Applications of microanalytical techniques to understanding mineralizing processes. *Reviews in Economic Geology,* **7**. 1-35.